Archives of Biochemistry and Biophysics 770 (2025) 110479

Contents lists available at ScienceDirect

Archives of Biochemistry and Biophysics

journal homepage: www.elsevier.com/locate/yabbi

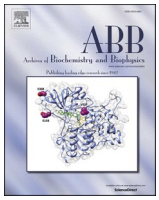

Crystal structures of the phosphorylation mimics of human cytosolic branched chain aminotransferase

Elizabeth S. Dare [a], Robert H. Newman [b], Myra E. Conway [c], Ming Dong [a,*]

[a] Department of Chemistry and Biochemistry, University of North Carolina Wilmington, Wilmington, NC, USA
[b] Department of Biology, North Carolina A&T State University, Greensboro, NC, USA
[c] College of Health, Psychology and Social Care, University of Derby, Derby, UK

ARTICLE INFO

Keywords:
hBCATc
CXXC motif
Interdomain loop
Transaminase
Phosphorylation

ABSTRACT

The phosphorylation sites of the human cytosolic Branched Chain Aminotransferase (hBCATc) mediated by mitogen-activated protein kinase (MAPK)/extracellular-signal-regulated-kinase 2 (ERK2, also known as MAPK1) were mapped. The crystal structures of the phosphorylation mimics at T33 and T36 were determined. The modified transaminase activity of these variants was analyzed. Although there were no major conformational changes in the phosphorylation mimics of hBCAT, a regional conformational change at the interdomain loop was observed mainly in mutant T33E. Consistently, when the catalytic turnovers of the T33E and T36E mutants were comparable to the wild type of hBCATc, the K_M dropped significantly compared to the wild type, indicating a shift of the substrate binding affinity in the mutants. Taken together, this indicated the phosphorylation of hBCATc by ERK2 is affecting the hBCATc's transaminase activity.

1. Introduction

The human cytosolic Branched Chain Aminotransferase (hBCATc) catalyzes the transamination of the branched chain amino acids and α-ketoglutarate to their respective α-keto acids and glutamate. The hBCAT proteins are PLP-dependent enzymes and the reaction is accompanied by conversion of the cofactor pyridoxal 5′-phosphate (PLP) and pyridoxamine 5′-phosphate (PMP) [1–4]. Importantly, hBCATc has a unique regulatory CXXC motif, located approximately 10 Å from the active site. This redox active CXXC motif (C335XXC338) undergoes recycling between its reduced and oxidized state, switching from active to less active, respectively [5–9]. Previous crystallographic studies have shown that oxidation of the catalytic cysteine changes the conformation of the interdomain loop (residues 191–201) that influences substrate binding, as well as a loop near the N-terminus (residues 35–52), disrupting the integrity of the substrate binding pocket and regulating hBCATc activity [10,11].

The canonical mitogen-activated protein kinase (MAPK) family member, extracellular-signal-regulated-kinase 2 (ERK2, also known as MAPK1), regulates many cellular processes through phosphorylating transcription factors, cytoskeletal proteins and other protein kinases and enzymes [12–17]. This pathway has also been implicated in the pathogenesis of many diseases including cancers [18], Type II diabetes [19], and cardiovascular disease [20,21]. As a critical kinase in cell growth and proliferation signaling pathways, the ERK2 protein needs to be diphosphorylated (pT185 and pT187) by its upstream kinase, MAP-K/ERK kinase 1 (MEK1), to become activated [12,22–24]. Recently, hBCATc has been shown to regulate serine/threonine-protein kinase (Akt) and ERK2, in the context of in cell proliferation and migration in triple negative breast cancer (TNBC). In that study, our team showed a redox regulated phosphorylation of hBCATc mediated by ERK2 [25] as a novel target of ERK2. Interestingly, this is not a one-way regulation. For instance, in the TNBC cells, overexpression of hBCATc negatively regulates the phosphorylation of ERK2 in MDA-MD-231 cells.

Previously hBCATc has been shown to be upregulated in a variety of cancers including liver cancer [26], glioma cancer [27], ovarian cancer [28], and breast cancer [29]. With ERK2 shown to regulate many cellular processes, the observed interplay between ERK2 and hBCATc opens new areas of investigation. For example, what site(s) on hBCATc is phosphorylated by ERK2 and what is the consequence of ERK2-mediated phosphorylation of hBCATc? Likewise, does phosphorylated hBCATc still have transaminase activity and where are the phosphorylation sites? Interestingly, in the previous study, hBCATc was also shown to activate the PI3K/Akt pathway, while inhibiting ERK2

* Corresponding author.
E-mail address: dongm@uncw.edu (M. Dong).

https://doi.org/10.1016/j.abb.2025.110479
Received 23 April 2025; Received in revised form 20 May 2025; Accepted 22 May 2025
Available online 23 May 2025

activation/phosphorylation, which identified hBCATc as a novel regulator of cell proliferation by regulating the PI3K/Akt and Ras/ERK pathways [25].

Functionally, both hBCATc and ERK2 are redox regulated for their respective activities [5,30,31] [11,24]. The redox center of hBCATc contains C335 and C338 which, when oxidized from dithiol to disulfide, lower transaminase activity [6,8]. ERK2 contains C159 in one of the substrate recognition sites, and its redox status variably regulates ERK's affinity for numerous substrates. Specifically, ERK2 was shown to be sulfenylated on C159 which is within its D-recruitment site surface (DRS) ligand binding domain, and oxidation in vitro was shown to differentially alter ERK2's activity toward various substrates of ERK2, with some substrates exhibiting decreased affinity and others an increase in affinity for oxidized ERK2 [24]. Additional results have shown that the phosphorylation of hBCATc mediated by ERK2 is redox regulated, where the phosphorylation is decreased when hBCATc is oxidized [25].

This paper focuses on the consequences of hBCATc phosphorylation mediated by ERK2. The sites of hBCATc phosphorylation by ERK2 were mapped, crystal structures were determined for two hBCATc variants mimicking phosphorylation at two of these sites (T33E and T36E), and transaminase activity of these variants was analyzed. This is the first structural and functional study on phosphorylation regulation of a PLP-dependent enzyme BCAT.

2. Materials and methods

2.1. Protein expression and purification

The expression and purification of hBCATc wild type and mutants (T33E, T36E) were carried out as previously described [32]. The hBCATc cDNA clone was ligated into the pET-28a expression vector with a N-terminal his-tag and subsequently used to transform BL21 (DE3) cells and induced with 1 mM Isopropyl β-D-1-thiogalactopyranoside (IPTG). Site-directed mutagenesis was performed with forward and reverse primers (**Supplemental materials**). Glycerol stock of BL21 cells that contains hBCAT plasmids was used to initiate inoculation in 200 mL LB with 50 μg/mL of kanamycin for 16 h at 37 °C, followed by being transferred into 3.6 L LB with 50 μg/mL of kanamycin for another 6–9 h or until OD600 reading reached 0.6. Expression was induced with 1 mM isopropyl-D-thiogalactopyranoside (IPTG). After 8 h at 30 °C, 180 RPM, cells were then harvested and pelleted at 10000×*g* for 15 min at 4 °C. The cell pellet was then suspended in extraction buffer which contains 0.1 M sodium phosphate, pH 8.0, 0.01 M Tris-HCl, 5 mM β-mercaptoethanol. The mixture was then sonicated for 5 s on and 10 s off for 1 min for 10 times. The cell extract was then centrifuged for 10 min at 7800×*g* at 4 °C. Clear supernatant was collected and then loaded onto 10 mL of Nickel-NTA resin which was already equilibrated in the extraction buffer. The column was then washed sequentially with a series of buffers with 5 column volumes of each of them (**Supplemental materials**). Each wash was retained, and an aliquot was taken for SDS-PAGE analysis. The final purification step of BCAT protein was via anion-exchange chromatography (macro-prep high Q from Biorad) which was pre-equilibrated in 10 mM potassium phosphate, pH 8.0. The proteins were then eluted selectively using a sodium chloride gradient from 100 mM to 1 M in 10 mM potassium phosphate, pH 8.0 over 20 min at a flow rate of 1.0 mL/min. The purified proteins are then dialyzed at 4 °C into storage buffer containing 25 mM Tris-HCl at pH 7.5, 150 mM NaCl, 5 mM DTT [33]. The hBCATc protein was then concentrated to 20 mg/mL, aliquoted in 50 μL, flash frozen, and stored at −80 °C. Protein concentration was estimated with absorbance at 280 nm using extinction coefficient of 67,600 $M^{-1}cm^{-1}$ per monomer.

2.2. LC/MS analysis of the hBCATc phosphorylation sites

The hBCATc was phosphorylated by activated ERK2 (purchased from SignalChem) in a master-mix buffer including 25 mM MOPS pH 7.2 buffer, 10 mM Beta-glycerol phosphate, 20 mM $MgCl_2$, 4 mM EGTA, 1.6 mM EDTA, 0.2 mM DTT, 100 ng/μL BSA, and 100 μM ATP. BCAT and ERK2 had had a concentration of 50 μM and 0.5 μM respectively. Negative controls contained BCAT only and buffer only. After being incubated for 1 h at 30 °C, the sample were ready for LC-MS/MS analysis [34–36]. Protein samples were reduced and alkylated in the presence of 10 mM dithiothreitol with 30 mM iodoacetamide, which was precipitated by incubation at −20 °C overnight with an addition 4X the sample volume of cold acetone. Following centrifugation at 14,000×*g* for 10 min, the pellet was air-dried at room temperature and then re-suspended in 50 mM ammonium bicarbonate using a cell disruptor to obtain a homogeneous suspension. Sequencing grade modified trypsin was added to the sample which was incubated at 37 °C overnight for enzymatic cleavage. The peptide solution was acidified using formic acid to quench the enzyme reaction and subsequently purified using a C18 spin tip and dried. Peptides were then prepared in 5 % (v/v) ACN containing 1 % (v/v) formic acid for LC-MS/MS analysis.

Samples were analyzed on a LC-MS/MS system (Orbitrap Velos Pro Mass Spectrometer (Thermo Scientific, Waltham, MA)) and a Dionex Ultimate-3000 nano-UPLC system (Thermo Scientific, Waltham, MA). An Acclaim PepMap 100 (C18, 5 μm, 100 Å, 100 μm × 2 cm) trap column and an Acclaim PepMap RSLC (C18, 2 μm, 100 Å, 75 μm × 50 cm) analytical column were employed for peptide separation. MS spectra were acquired by data-dependent scans consisting of MS/MS scans of the ten most intense ions from the full MS scan with dynamic exclusion option (30 s). To identify proteins, spectra were searched against human BCAT1 protein sequence (UniProtKB, Oct 2021) using Sequest HT algorithm within the Proteome Discoverer v2.5 (Thermo Scientific, Waltham, MA). Search parameters were as follows: FT-trap instrument, parent mass error tolerance of 10 ppm, fragment mass error tolerance of 0.6 Da (monoisotopic); enzyme, trypsin (full); number of max missed cleavages; variable modifications, +15.995 Da (oxidation) on M, +79.966 Da (phosphorylation) on S, T, and Y, +42.011 Da (acetyl) on protein N-term.

2.3. Crystallization and data collection

The T33E, T36E mutants of hBCATc were subjected to sparse-matrix crystallization screening using the hanging-drop vapor diffusion method. Screening kits from Hampton Research were used for the screening. A well solution of 225 mM $MgCl_2$ with 16–20 % PEG 3350 was optimized to form crystals. Crystals were cryoprotected by transferring to well solutions with 20 % glycerol for 1 min before flash freezing. Frozen crystals were then transferred to the SLAC synchrotron facility where diffraction data were collected. The diffraction data were collected at 100 K on the beamline of SSRL Beamline BL12-2 with a wavelength of 0.97956 Å, and the detector is Dectris Eiger 2 x 16 M.

2.4. Structure determination and refinements

The diffraction data were indexed, integrated and scaled using AutoXDS [37]. MOLREP from CCP4 (Bailey, 1994) was used for molecular replacement using hBCATc wild type structure [38] (PDB entry:2coj) as a search model. The models were built by replacing both T33 and T36 with E. The coordinates were refined *via* REFMAC5 from CCP4 [39] and COOT [40]. The final model composed of PLP, two monomers and water molecules. The UCSF CHIMERA was used to present the structures [41].

2.5. Steady-state kinetics analysis

The hBCATc activity was measured by coupling the transamination reaction of L-Leu with α-ketoglutarate producing α-Ketoisocaproic acid (KIC) catalyzed by hBCATc, with another reductive amination reaction catalyzed by Leucine Dehydrogenase (Leu-DH) with substrates of KIC,

ammonia and NADH where KIC was reduced back to L-Leucine [42]. The volume of the reaction was 100 μL and the path length was 0.2 cm in the activity assay. The reaction rate was monitored at 340 nm by the continuously decreased concentration of NADH to NAD^+. The reaction buffer contained 50 mM Tris pH 7.5, 25 mM ammonium sulfate, 0.125–10 mM L-Leu, 0.25 mM NADH, 0.005 mM of PLP, 5 mM of ketoglutarate, and 2.5 mM of DTT.

2.5.1. Data availability

The pdb deposits (pdb codes: 9FBA, 9FBO) can be found at www.rcsb.org. The mass spectrometry proteomics data have been deposited to the ProteomeXchange Consortium via the PRIDE [43] partner repository with the dataset identifier PXD062954. The initial velocity stead-state kinetics data can be shared upon request.

3. Results

We mapped the ERK2-mediated phosphorylation sites of hBCATc which are T33, T36, S341, and Y345, with T33 and T36 near the N-terminus and S341 close to the redox center (C335 and C338) (Fig. 1). Previously the N-terminal loop including T33 and T36 was shown to affect the hBCATc activity as transaminase [9]. Focusing on the N-terminal phosphosites, plasmids for expression of variants T33E and T36E were prepared to mimic the phosphorylated proteins and determine their structural and functional features. Both mutants were overexpressed in *E. coli* BL21 cells and purified with affinity (Ni-NTA) and anion exchange chromatography.

Crystallization conditions were screened and optimized to obtain crystals of 20–50 μm. Crystals of the T33E mutant formed on day three in thin and square shapes. For the T36E mutant, needle-shaped crystals of T36E mutant were obtained on day two and larger, squared-shaped crystals were obtained after seeding. The diffraction data were collected at the SLAC synchrotron, then processed and scaled using XDS and AUTO PROC [37]. High-quality crystals of both variants were obtained as the T33E mutant diffracts to 1.78 Å and the T36E mutant diffracts to 1.66 Å. Both crystals have a space group of orthorhombic space group $P2_12_12_1$ but different cell dimensions. Data collection statistics are presented in Table 1.

The structures of both T33E and T36E mutants resemble the canonical wild type hBCATc homodimer (pdb: 2coj; exhibiting RMSD:0.677 Å and 0.578 Å, respectively). Likewise, in both structures, a Schiff-base linked PLP was observed in the active sites linked to K222 (Fig. 2) and the CXXC center of the mutants remained reduced similar to

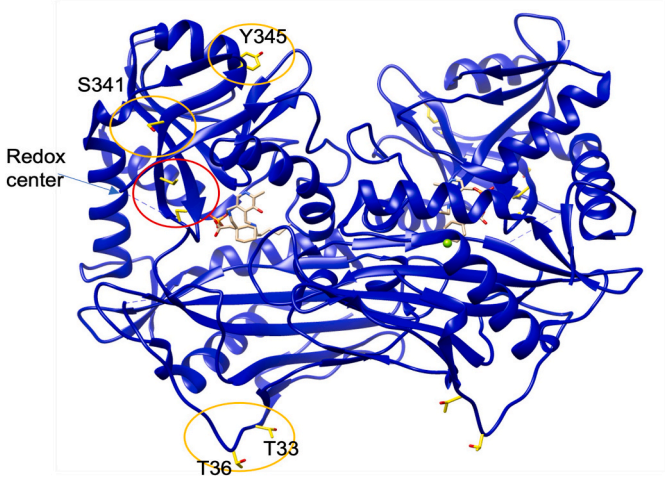

Fig. 1. The phosphorylation sites of hBCATc by ERK2 were confirmed with LC-MS/MS. The sites are T33, T36, S341 and Y345 (circled in orange). The redox center is labelled (circled in red). The PLP is circled in green. Crystal structure of hBCATc was used to map the phosphorylation sites (pdb: 2coj).

Table 1
Crystal structure parameters.

	T33E	T36E
Wavelength (Å)	0.97946	0.97946
Temperature (K)	100	100
Detector	Dectris Eiger2 x 16 M	Dectris Eiger2 x 16 M
Space group	$P2_12_12_1$	$P2_12_12_1$
Unit cell dimensions a, b, c (Å), α, β, γ (°)	110.284, 115.63, 149.413 90.0, 90.0, 90.0	66.962, 106.896, 110.477 90.0, 90.0, 90.0
Resolution (Å)	91.445–1.786	76.822–1.663
Completeness (%)	99.9 (99.9)	92.8 (99.8)
Redundancy	12.1	11.4
I/σI	6.3	9.5
$CC_{1/2}$	0.996	0.986
No. of unique reflections	180795 (8983)	86971 (4594)
pdb code	9FBA	9FBO
Resolution range (Å)	91.4–1.78	76.8–1.66
No. of reflections, test set	7330	3961
Final R_{cryst}	0.232	0.2046
Final R_{free}	0.267	0.246
R.M.S. deviations		
Bonds(Å)	0.0068	0.0089
Angles (°)	1.66	1.87
Average B factors (Å^2)	31.637	33.482
Ramachandran plot favored region (%)	99	97
Favored region (%)	97	97
Additionally allowed (%)	3	3
Outliers (%)		

the wild type protein. The substrate binding pocket includes residues Y161, R163, Y227, K222, T260 from the same monomer and Y90, V175 from the other monomer within the homodimer, which are consistent with the structure of wild type hBCATc (Fig. 2). However, there is a conformational change of the interdomain loop (residues 191–201) in both mutants, which is more prominent in mutant T33E (Figs. 2 and 3). For instance, Y193 was in close contact with C335, A334, F49 and F194 in the wild type, but this close contact with F194 (6.6 Å) was not observed in the T33E mutant (12.9 Å) due to a large conformational change in the interdomain loop (Fig. 3). In the T33E mutant, Y193 moved away from the active site by about 4.8 Å (Fig. 3) compared to the wild type protein, widening the access channel to the active site (**SF.1**). For the T36E mutant, the interdomain loop was mostly disordered, but the conformation of residue P192 more closely resembles that of the P192 in T33E than it does wild type, suggesting that Y193 in T33E also adopts a similar conformation to that observed in T36E (Fig. 3, **SF.2**). The N-terminal loop (residues 35–52) in both the T33E and T36E mutants overlays well with the wild type hBCATc (Fig. 2), apart from A46 from wild type (pdb: 2coj) (not shown in the structure), potentially as a result of high flexibility.

Steady state kinetic analysis showed that both T33E and T36E mutants have lower but comparable k_{cat} values, and a decreased K_M (close to 10-fold) compared to the wild type, which led to higher catalytic efficiency values compared to the wild type hBCATc (Fig. 4 and Table 2). The K_M value determined here for the wild type protein is consistent with that from previous work [32].

4. Discussion

There was no overall structural change when the T33E and T36E mutants were compared to WT BCATc However, the interdomain loop (residues 191–201), which was previously shown to affect substrate binding by modulating access to the active site [7,9], did incur conformational changes. More specifically, the interdomain loop (residues 191–201) which connects the small domain (N-terminus to residue V190) and the large domain (residue V202 to C-terminus) exhibited conformational changes in both mutants (Fig. 2). In the interdomain loop, the shift of Y193 away from the active site pocket observed in the

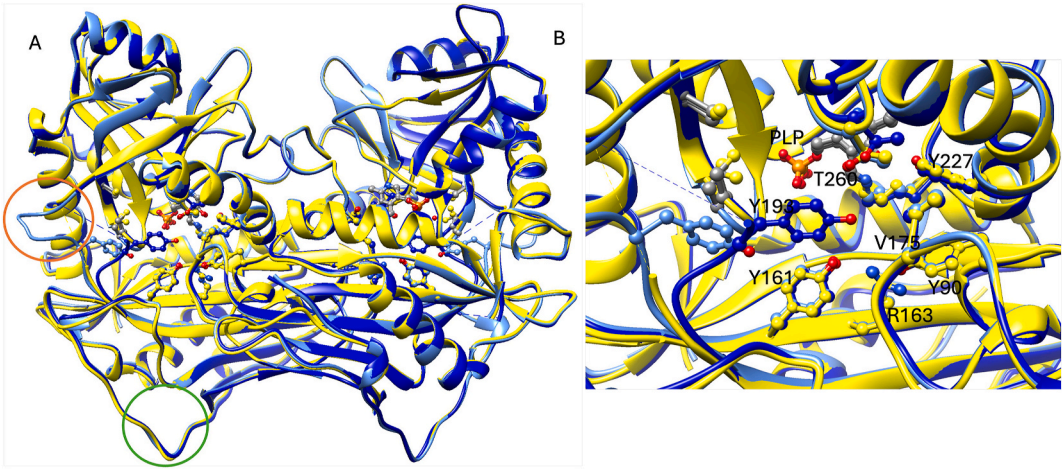

Fig. 2. A. The overlay of the wild type hBCATc (colored in dark blue) and the T33E (colored in light blue), and T36E (colored in yellow). The interdomain loop is circled in orange. The N-terminal domain is circled in green. B. The close-up of the active site including Y193, T260, Y227, V175, Y161, Y90 and R163.

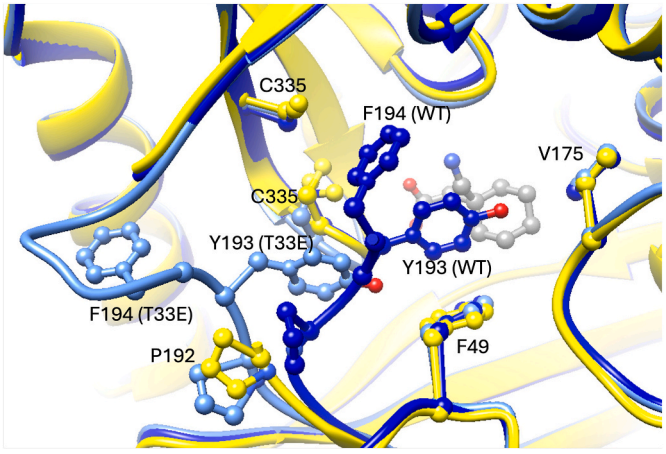

Fig. 3. The close-up of the interdomain loop overlay of the wild type (shown in blue), T36E (show in yellow) and T33E (shown in light blue). The P192 residue in both mutants had shifted coordinates for 3.4–5 Å compared to the wild type. The F194 of T33E residues had a shifted away from the active site for 14 Å compared to where it was in the wild type. The Y193 in the T33E shifted away from the active site for about 4.8 Å. The inhibitor gabapentin which resides the active site is shown in grey.

crystal structure of the T33E mutant led to widened access for substrates to bind to the active site of hBCATc. Consequently, the distance between the phenyl ring of Y193 and Cβ of C335 decreased from 5.8 Å in wild type to 3.6 Å in T33E, and the distance between the hydroxyl group of Y193 and the sulfur of C335 decreased from 7.9 Å in wild type to 6.2 Å in T33E (**SF.3**). Consistent with this observation, it was previously proposed that the C315 thiol group in the reduced redox center of the mitochondrial isoform, hBCATm (corresponding to C335 in hBCATc), interacts with the interdomain loop and stabilizes Y173 (corresponding to Y193 in hBCATc), impacting catalysis [5]. Based on these new data, we postulate a model in which ERK2-mediated phosphorylation of the N-terminus of hBCATc at one or both sites (T33 and T38) leads to conformational changes in the interdomain loop which consequently affect the catalytic efficiency. In addition to the previously well-established regulation through oxidation status of C335 and C338 in the redox center, this model adds another layer of hBCATc regulation that depends on post translational modifications (PTMs) at the N-terminus of the protein. The T33E mutant revealed a change in the conformation of P192 and Y193 in the interdomain loop which was also likely reflected in changes observed in the T36E mutant, although the latter was more disordered from residues Y193 (Fig. 3).

The observed elevated catalytic efficiencies (k_{cat}/K_M) of T33E and T36E mutants compared to wild type hBCATc suggested that ERK2-mediated phosphorylation of hBCATc on T33 and/or T36 increases hBCATc's transaminase catalytic efficiency. Interestingly, the single phosphorylation mimic had a similar impact on the k_{cat} and K_M of hBCATc as the double mutant. More specifically, the k_{cat} and K_M values we observed for the double mutant are intermediate between those of the two single mutants. One postulate is that the phosphorylation at either site is sufficient to induce a conformational shift that affects the catalytic efficiency and substrate binding, and the double mutant doesn't provide any further effect than what a single phosphorylation achieves. Another possibility is that the k_{cat} and K_M of the double mutant reflects a combination of the single mutants' effects on the k_{cat} and K_M.

Previously, oxidation of the redox-active CXXC motif was shown to regulate the activity of hBCATc by triggering a conformational change in the interdomain and N-terminal loops [9]. Our study shows increased transaminase catalytic efficiencies due to added negative charges through mutations near the N-terminus (T33E and T36E mutant proteins), both of which are approximate mimics of the phosphorylated hBCATc modified by ERK2. This result further supported that the conformation and modification status of the N-terminus of hBCATc regulates the transaminase activity, with phosphorylation potentially enhancing the binding of the substrate at the active site pocket as suggested by the observed decreased K_M values in the T33E and T36E mutants. This work with hBCATc provides the first evidence for allosteric regulation of a fold type IV aminotransferase [44,45]. This suggests therapeutic targets on BCAT proteins other than the CXXC motif, which will ultimately provide new avenues for drug discovery for BCAT regulation.

Branch chain amino acids (BCAAs) such as leucine, isoleucine, and valine play important roles in cancer metabolism and progression [46–48]. Leucine, one of BCAT's substrates, has been shown to affect mTORC1 and Akt pathways [48–50]. Since BCAT is one key enzyme regulating Leu concentration in cytosol, the observed a higher catalytic efficiency of phosphorylated hBCATc (modified by ERK2 and mimicked in the T33E and T36E mutants) could have an impact on cytosolic Leu concentration in cancer cells. Since transaminases play significant roles in amino acid metabolism and whole-body nitrogen shuttling, in particular with respect to the *de novo* synthesis of the neurotransmitter glutamate in the brain [51], the elevated transaminase activities imparted by ERK2-mediated phosphorylation could lead to a higher level of glutamate in the brain. Further cell-based work on the impacts of the phosphorylation-regulated activity of hBCATc will be needed.

The phosphomimetic mutants were used in this study to access the

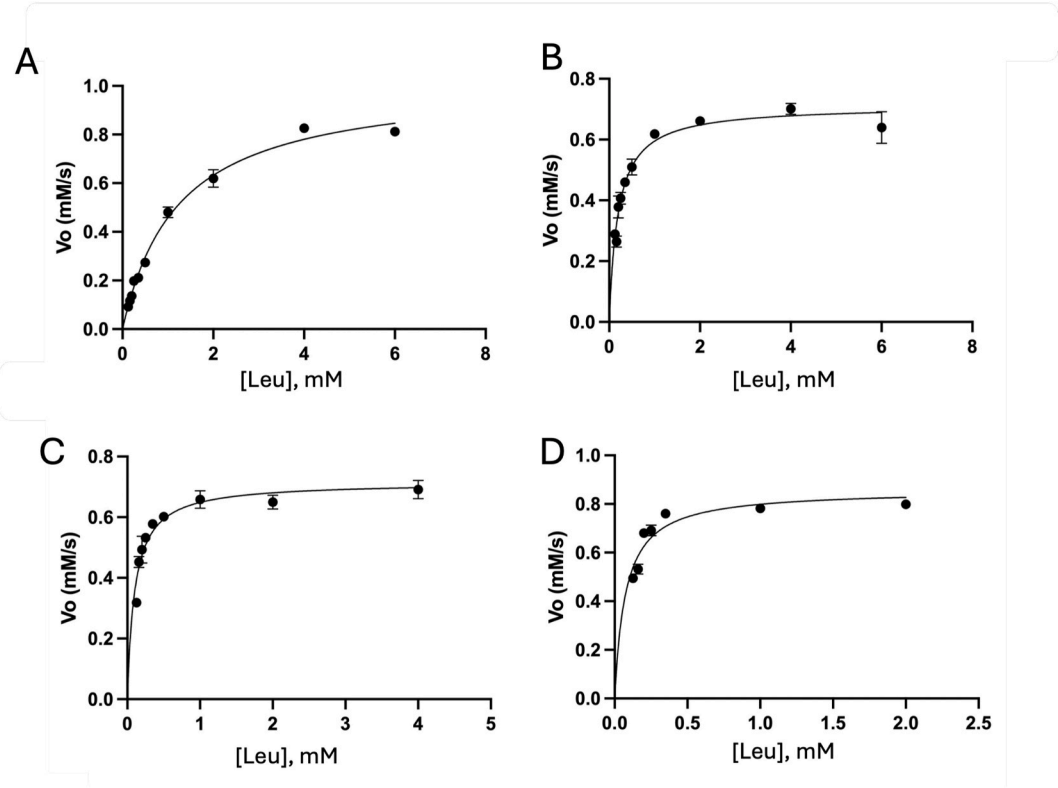

Fig. 4. The steady-state kinetics analysis of the BCAT wild type (A) and phosphorylation mimics of T33E (B), T36E (C) and T33/36E (D).

Table 2
Steady State study on hBCATc WT and phosphorylation mimic mutations.

	KM (mM)	kcat (s-1)	kcat/KM (mM-1s-1)
WT	1.2 ± 0.03	595 ± 9	487
T33E	0.17 ± 0.02	204 ± 7	1190
T36E	0.06 ± 0.02	371 ± 8	6180
T33/36E	0.08 ± 0.003	273 ± 3	3410

phosphorylation impacts on the activity of BCAT. While it has been acknowledged that they may not fully replicate the effects of true phosphorylation, phosphomimetics are still widely used and can provide important insights [52,53]. Future work will focus on directly purifying phosphorylated BCAT for structural and functional analysis.

Overall, this work entailed mapping of the phosphorylation sites of hBCATc by ERK2 and investigation of the impact of ERK2-mediated phosphorylation on hBCATc transaminase activity. Our structural and functional results suggested that the phosphorylation of hBCATc mediated by ERK2 affects the catalytic efficiency of hBCATc by changing the conformation of the interdomain loop. A new allosteric regulation mechanism model for BCAT was proposed in this paper, providing new therapeutic strategies to regulate BCAT. These data, together with our previous work on the hBCATc reciprocally regulating ERK2 activation/phosphorylation, showed further evidence of an interplay of hBCATc and ERK2, both of which have been previously found to be highly expressed in breast cancer cells [29,54]. Although there is still much to be further explored about the structural, biochemical and cellular implications of the interplay between hBCATc and ERK2, these studies clearly demonstrate a functional connection between hBCATc and ERK2 that could impact a variety of disorders, including cancer, diabetes, and cardiovascular disease. Future structural and functional analyses on the protein-protein interactions of BCAT and ERK2 in various states are needed to have a clearer mechanistic understanding of their influence on one another.

CRediT authorship contribution statement

Elizabeth S. Dare: Investigation. **Robert H. Newman:** Writing – review & editing. **Myra E. Conway:** Writing – review & editing. **Ming Dong:** Writing – review & editing, Writing – original draft, Supervision, Methodology, Investigation, Formal analysis, Conceptualization.

Acknowledgements

The research was supported by NIH awards (SC2GM132050 to MD, 1R35GM153737 and 1SC1GM130545 to RHN), NSF award (2401097) to MD, and the UNCW Startup fund to MD. We would like to acknowledge the support provided by the Proteomics and Metabolomics Shared Resource of the Wake Forest School of Medicine and Wake Forest Baptist Comprehensive Cancer Center (NIH/NCI P30 CA12197). We would also like to thank Dr. Tzanko Doukov from SLAC for assisting us with the SLAC data collection. We would like to thank Aidan D. Holandez and Kameron J. Burton for producing the purified proteins.

Appendix A. Supplementary data

Supplementary data to this article can be found online at https://doi.org/10.1016/j.abb.2025.110479.

Data availability

Data will be made available on request.

References

[1] L. Birolo, E. Sandmeier, P. Christen, R.A. John, The roles of Tyr70 and Tyr225 in aspartate aminotransferase assessed by analysing the effects of mutations on the

multiple reactions of the substrate analogue serine o-sulphate, Eur. J. Biochem. 232 (3) (1995) 859–864.
[2] J. Jäger, M. Moser, U. Sauder, J.N. Jansonius, Crystal structures of Escherichia coli aspartate aminotransferase in two conformations. Comparison of an unliganded open and two liganded closed forms, J. Mol. Biol. 239 (2) (1994) 285–305.
[3] T. Yano, S. Kuramitsu, S. Tanase, Y. Morino, H. Kagamiyama, Role of Asp222 in the catalytic mechanism of Escherichia coli aspartate aminotransferase: the amino acid residue which enhances the function of the enzyme-bound coenzyme pyridoxal 5'-phosphate, Biochemistry 31 (25) (1992) 5878–5887.
[4] D.L. Smith, S.C. Almo, M.D. Toney, D. Ringe, 2.8-A-resolution crystal structure of an active-site mutant of aspartate aminotransferase from Escherichia coli, Biochemistry 28 (20) (1989) 8161–8167.
[5] M.E. Conway, N. Yennawar, R. Wallin, L.B. Poole, S.M. Hutson, Identification of a peroxide-sensitive redox switch at the CXXC motif in the human mitochondrial branched chain aminotransferase, Biochemistry 41 (29) (2002) 9070–9078.
[6] Myra E. Conway, Reidar Wallin, Leslie B. Poole, Susan M. Hutson, Identification of a peroxide-sensitive redox switch at the CXXC motif in the human mitochondrial branched chain aminotransferase, Biochemistry 41 (2002) 9070–9078.
[7] M.E. Conway, N. Yennawar, R. Wallin, L.B. Poole, S.M. Hutson, Human mitochondrial branched chain aminotransferase: structural basis for substrate specificity and role of redox active cysteines, Biochim. Biophys. Acta 1647 (1–2) (2003) 61–65.
[8] Myra E. Conway, Susan M. Hutson, Roles for cysteine residues in the regulatory CXXC motif of human mitochondrial branched chain, Aminotrans Biochem. 43 (2004) 7356–7364.
[9] M. Goto, I. Miyahara, K. Hirotsu, M. Conway, N. Yennawar, M.M. Islam, S. M. Hutson, Structural determinants for branched-chain aminotransferase isozyme-specific inhibition by the anticonvulsant drug gabapentin, J. Biol. Chem. 280 (44) (2005) 37246–37256.
[10] N.H. Yennawar, M.M. Islam, M. Conway, R. Wallin, S.M. Hutson, Human mitochondrial branched chain aminotransferase isozyme: structural role of the CXXC center in catalysis, J. Biol. Chem. 281 (51) (2006) 39660–39671.
[11] D. Herbert, S. Gibbs, A. Riddick, M. Conway, M. Dong, Crystal structure of an oxidized mutant of human mitochondrial branched-chain aminotransferase, Acta. Crystallogr. F Struct. Biol. Commun. 76 (Pt 1) (2020) 14–19.
[12] Y. Mebratu, Y. Tesfaigzi, How ERK1/2 activation controls cell proliferation and cell death: is subcellular localization the answer? Cell Cycle 8 (8) (2009) 1168–1175.
[13] M. Zakrzewska, E.M. Haugsten, B. Nadratowska-Wesolowska, A. Oppelt, B. Hausott, Y. Jin, J. Otlewski, J. Wesche, A. Wiedlocha, ERK-mediated phosphorylation of fibroblast growth factor receptor 1 on Ser777 inhibits signaling, Sci. Signal. 6 (262) (2013) ra11.
[14] J.D. Keyes, D. Parsonage, R.D. Yammani, L.C. Rogers, C. Kesty, C.M. Furdui, K. J. Nelson, L.B. Poole, Endogenous, regulatory cysteine sulfenylation of ERK kinases in response to proliferative signals, Free Radic. Biol. Med. 112 (2017) 534–543.
[15] S. Han, Y. Ren, W. He, H. Liu, Z. Zhi, X. Zhu, T. Yang, Y. Rong, B. Ma, T.J. Purwin, Z. Ouyang, C. Li, X. Wang, X. Wang, H. Yang, Y. Zheng, A.E. Aplin, J. Liu, Y. Shao, ERK-mediated phosphorylation regulates SOX10 sumoylation and targets expression in mutant BRAF melanoma, Nat. Commun. 9 (1) (2018) 28.
[16] S.M. Soond, B. Everson, D.W. Riches, G. Murphy, ERK-mediated phosphorylation of Thr735 in TNFalpha-converting enzyme and its potential role in TACE protein trafficking, J. Cell Sci. 118 (Pt 11) (2005) 2371–2380.
[17] R.A. Saxton, D.M. Sabatini, mTOR signaling in growth, metabolism, and disease, Cell 168 (6) (2017) 960–976.
[18] P.J. Roberts, C.J. Der, Targeting the Raf-MEK-ERK mitogen-activated protein kinase cascade for the treatment of cancer, Oncogene 26 (22) (2007) 3291–3310.
[19] J. Hirosumi, G. Tuncman, L. Chang, C.Z. Görgün, K.T. Uysal, K. Maeda, M. Karin, G.S. Hotamisligil, A central role for JNK in obesity and insulin resistance, Nature 420 (6913) (2002) 333–336.
[20] A.J. Muslin, MAPK signalling in cardiovascular health and disease: molecular mechanisms and therapeutic targets, Clin. Sci. (Lond.) 115 (7) (2008) 203–218.
[21] Y. Wang, Mitogen-activated protein kinases in heart development and diseases, Circulation (New York, N. Y.) 116 (12) (2007) 1413–1423.
[22] A.C. McReynolds, A.S. Karra, Y. Li, E.D. Lopez, A.G. Turjanski, E. Dioum, K. Lorenz, E. Zaganjor, S. Stippec, K. McGlynn, S. Earnest, M.H. Cobb, Phosphorylation or mutation of the ERK2 activation loop alters oligonucleotide binding, Biochemistry 55 (12) (2016) 1909–1917.
[23] B.J. Canagarajah, A. Khokhlatchev, M.H. Cobb, E.J. Goldsmith, Activation mechanism of the MAP kinase ERK2 by dual phosphorylation, Cell 90 (5) (1997) 859–869.
[24] A.E. Postiglione, L.L. Adams, E.S. Ekhator, A.E. Odelade, S. Patwardhan, M. Chaudhari, A.S. Pardue, A. Kumari, W.A. LeFever, O.P. Tornow, T.S. Kaoud, J. Neiswinger, J.S. Jeong, D. Parsonage, K.J. Nelson, D.B. Kc, C.M. Furdui, H. Zhu, A.J. Wommack, K.N. Dalby, M. Dong, L.B. Poole, J.D. Keyes, R.H. Newman, Hydrogen peroxide-dependent oxidation of ERK2 within its D-recruitment site alters its substrate selection, iScience 26 (10) (2023).
[25] T.F. Mai Ahmed Shafei, Jasmine Davis, Arwa Flemban, David Qualtrough, Sarah Dean, Claire Perks, Ming Dong, Robert Newman, Myra Elizabeth Conway, BCATc modulates crosstalk between the PI3K/Akt and the Ras/ERK pathway regulating proliferation in triple negative breast cancer, Oncotarget 11 (2020).
[26] M. Xu, Q. Liu, Y. Jia, K. Tu, Y. Yao, Q. Liu, C. Guo, BCAT1 promotes tumor cell migration and invasion in hepatocellular carcinoma, Oncol. Lett. 12 (4) (2016) 2648–2656.
[27] M. Tonjes, S. Barbus, Y.J. Park, W. Wang, M. Schlotter, A.M. Lindroth, S.V. Pleier, A.H.C. Bai, D. Karra, R.M. Piro, J. Felsberg, A. Addington, D. Lemke, I. Weibrecht, V. Hovestadt, C.G. Rolli, B. Campos, S. Turcan, D. Sturm, H. Witt, T.A. Chan, C. Herold-Mende, R. Kemkemer, R. Konig, K. Schmidt, W.E. Hull, S.M. Pfister, M. Jugold, S.M. Hutson, C. Plass, J.G. Okun, G. Reifenberger, P. Lichter, B. Radlwimmer, BCAT1 promotes cell proliferation through amino acid catabolism in gliomas carrying wild-type IDH1, Nat. Med. 19 (7) (2013) 901–908.
[28] A.F. Zhi-Qiang Wang, Magdalena Bachvarova, Marie Plante, Jean Gregoire, Marie-Claude Renaud, Alexandra Sebastianelli, Chantal Guillemette, Stéphane Gobeil, Elizabeth Macdonald, Barbara Vanderhyden, Dimcho Bachvarov, BCAT1 expression associates with ovarian cancer progression: possible implications in altered disease metabolism, Oncotarget 6 (31) (2015).
[29] V. Thewes, R. Simon, M. Hlevnjak, M. Schlotter, P. Schroeter, K. Schmidt, Y. Wu, T. Anzeneder, W. Wang, P. Windisch, M. Kirchgassner, N. Melling, N. Kneisel, R. Buttner, U. Deuschle, H.P. Sinn, A. Schneeweiss, S. Heck, S. Kaulfuss, H. Hess-Stumpp, J.G. Okun, G. Sauter, A.E. Lykkesfeldt, M. Zapatka, B. Radlwimmer, P. Lichter, M. Tonjes, The branched-chain amino acid transaminase 1 sustains growth of antiestrogen-resistant and ERalpha-negative breast cancer, Oncogene 36 (29) (2017) 4124–4134.
[30] K. Traore, R. Sharma, R.K. Thimmulappa, W.H. Watson, S. Biswal, M.A. Trush, Redox-regulation of Erk1/2-directed phosphatase by reactive oxygen species: role in signaling TPA-induced growth arrest in ML-1 cells, J. Cell. Physiol. 216 (1) (2008) 276–285.
[31] M.E. Conway, L.B. Poole, S.M. Hutson, Roles for cysteine residues in the regulatory CXXC motif of human mitochondrial branched chain aminotransferase enzyme, Biochemistry 43 (23) (2004) 7356–7364.
[32] J. Davoodi, P.M. Drown, R.K. Bledsoe, R. Wallin, G.D. Reinhart, S.M. Hutson, Overexpression and characterization of the human mitochondrial and cytosolic branched-chain aminotransferases, J. Biol. Chem. 273 (9) (1998) 4982–4989.
[33] M.M. Islam, M. Nautiyal, R.M. Wynn, J.A. Mobley, D.T. Chuang, S.M. Hutson, Branched-chain amino acid metabolon: interaction of glutamate dehydrogenase with the mitochondrial branched-chain aminotransferase (BCATm), J. Biol. Chem. 285 (1) (2010) 265–276.
[34] M.J. Previs, P. VanBuren, K.J. Begin, J.O. Vigoreaux, M.M. LeWinter, D. E. Matthews, Quantification of protein phosphorylation by liquid chromatography-mass spectrometry, Anal. Chem. 80 (15) (2008) 5864–5872.
[35] K. Blackburn, M.B. Goshe, Challenges and strategies for targeted phosphorylation site identification and quantification using mass spectrometry analysis, Briefings Funct. Genomics Proteomics 8 (2) (2009) 90–103.
[36] F. Drepper, J. Biernat, S. Kaniyappan, H.E. Meyer, E.M. Mandelkow, B. Warscheid, E. Mandelkow, A combinatorial native MS and LC-MS/MS approach reveals high intrinsic phosphorylation of human Tau but minimal levels of other key modifications, J. Biol. Chem. 295 (52) (2020) 18213–18225.
[37] T. Doukov, D. Herschlag, F. Yabukarski, Obtaining anomalous and ensemble information from protein crystals from 220 K up to physiological temperatures, Acta. Crystallogr. D Struct. Biol. 79 (Pt 3) (2023) 212–223.
[38] N.H. Yennawar, M.E. Conway, H.P. Yennawar, G.K. Farber, S.M. Hutson, Crystal structures of human mitochondrial branched chain aminotransferase reaction intermediates: ketimine and pyridoxamine phosphate forms, Biochemistry 41 (39) (2002) 11592–11601.
[39] N. Collaborative Computational Project, The CCP4 suite: programs for protein crystallography, Acta. Crystallogr. D Biol. Crystallogr. 50 (Pt 5) (1994) 760–763.
[40] P. Emsley, B. Lohkamp, W.G. Scott, K. Cowtan, Features and development of coot, Acta Crystallogr. Sect. D Biol. Crystallogr. 66 (4) (2010) 486–501.
[41] E.F. Pettersen, T.D. Goddard, C.C. Huang, G.S. Couch, D.M. Greenblatt, E.C. Meng, T.E. Ferrin, UCSF Chimera—a visualization system for exploratory research and analysis, J. Comput. Chem. 25 (13) (2004) 1605–1612.
[42] A.J. Cooper, M. Conway, S.M. Hutson, A continuous 96-well plate spectrophotometric assay for branched-chain amino acid aminotransferases, Anal. Biochem. 308 (1) (2002) 100–105.
[43] Y. Perez-Riverol, C. Bandla, D.J. Kundu, S. Kamatchinathan, J. Bai, S. Hewapathirana, N.S. John, A. Prakash, M. Walzer, S. Wang, J.A. Vizcaíno, The PRIDE database at 20 years: 2025 update, Nucleic Acids Res. 53 (D1) (2025) D543–d553.
[44] T. Pavkov-Keller, G.A. Strohmeier, M. Diepold, W. Peeters, N. Smeets, M. Schürmann, K. Gruber, H. Schwab, K. Steiner, Discovery and structural characterisation of new fold type IV-transaminases exemplify the diversity of this enzyme fold, Sci. Rep. 6 (2016) 38183.
[45] R.T. Taylor, V. Shakespeare, W.T. Jenkins, Branched chain amino acid aminotransferase. IV. Kinetics of the transamination reactions, J. Biol. Chem. 245 (19) (1970) 4880–4885.
[46] E.A. Ananieva, A.C. Wilkinson, Branched-chain amino acid metabolism in cancer, Curr. Opin. Clin. Nutr. Metab. Care 21 (1) (2018) 64–70.
[47] D. Biswas, L. Slade, L. Duffley, N. Mueller, K.T. Dao, A. Mercer, S. Pakkiriswami, Y. El Hiani, P.C. Kienesberger, T. Pulinilkunnil, Inhibiting BCKDK in triple negative breast cancer suppresses protein translation, impairs mitochondrial function, and potentiates doxorubicin cytotoxicity, Cell Death Discov. 7 (1) (2021) 241.
[48] Y. Song, B. Zhao, Y. Xu, X. Ren, Y. Lin, L. Zhou, Q. Sun, Prognostic significance of branched-chain amino acid transferase 1 and CD133 in triple-negative breast cancer, BMC Cancer 20 (1) (2020) 584.
[49] E. Xu, B. Ji, K. Jin, Y. Chen, Branched-chain amino acids catabolism and cancer progression: focus on therapeutic interventions, Front. Oncol. 13 (2023) 1220638.
[50] X. Nong, C. Zhang, J. Wang, P. Ding, G. Ji, T. Wu, The mechanism of branched-chain amino acid transferases in different diseases: research progress and future prospects, Front. Oncol. 12 (2022) 988290.
[51] J.T. Cole, A.J. Sweatt, S.M. Hutson, Expression of mitochondrial branched-chain aminotransferase and α-keto-acid dehydrogenase in rat brain: implications for neurotransmitter metabolism, Front. Neuroanat. 6 (2012) 18.
[52] T. Cesaro, Y. Hayashi, F. Borghese, D. Vertommen, F. Wavreil, T. Michiels, PKR activity modulation by phosphomimetic mutations of serine residues located three

aminoacids upstream of double-stranded RNA binding motifs, Sci. Rep. 11 (1) (2021) 9188.
[53] A. Tariq, J. Lin, M.M. Noll, M.P. Torrente, K.L. Mack, O.H. Murillo, M.E. Jackrel, J. Shorter, Potentiating Hsp104 activity via phosphomimetic mutations in the middle domain, FEMS Yeast Res. 18 (5) (2018).
[54] C. Bartholomeusz, A.M. Gonzalez-Angulo, P. Liu, N. Hayashi, A. Lluch, J. Ferrer-Lozano, G.N. Hortobágyi, High ERK protein expression levels correlate with shorter survival in triple-negative breast cancer patients, Oncologist 17 (6) (2012) 766–774.